JOURNAL OF APPLIED ELECTROCHEMISTRY 24 (1994) 751–757

Oxygen trickle-bed electrode as a cathode for chlor-alkali electrolysis

O. ŠPALEK

Institute of Inorganic Chemistry, Academy of Sciences of the Czech Republic, 160 00 Prague 6, Czech Republic

Received 17 July 1992; revised 4 December 1993

An experimental study of the oxygen trickle-bed electrode as a cathode for chlor-alkali membrane electrolysis is presented. The effects of gas and electrolyte flow rates, pressure, and the effect of electrode particle size on pressure drop, liquid holdup and cathode polarization have been studied. The experimental results are interpreted by means of equations characterizing pressure drop, liquid hold-up and oxygen mass transfer rate.

List of symbols

a surface area of spherical particles per unit electrode volume, $1.414.\pi/\bar{d}$ (m^{-1})
c_0 oxygen solubility in electrolyte ($mol\,m^{-3}$)
d effective particle diameter (m)
$\bar{d}$ mean particle size (m)
D oxygen diffusion coefficient ($m^2\,s^{-1}$)
E local potential in the electrode (V)
E' potential including the voltage loss $\Delta\phi$ (V)
f_p roughness factor of particle surface
g gravitational constant ($m\,s^{-2}$)
Ga Galileo number
h density ($kg\,m^{-3}$)
j superficial current density ($A\,m^{-2}$)
j_{lim} mass transfer controlled current density ($A\,m^{-2}$)
K_G mass transfer coefficient for gas phase ($m\,s^{-1}$)
K_L mass transfer coefficient for liquid between the gas-liquid interface and liquid bulk ($m\,s^{-1}$)
K_S mass transfer coefficient for liquid between liquid bulk and liquid-solid interface ($m\,s^{-1}$)
K_0 overall mass transfer coefficient ($m\,s^{-1}$)
ΔP pressure drop ($Pa\,m^{-1}$)
Re Reynolds number, $ud'h/\mu(1-\epsilon)$
Sc Schmidt number, μ/hD
t electrode thickness (m)
U linear velocity related to the empty cross section ($m\,s^{-1}$)
x distance from the current collector (m)

Greek symbols
β_1 transient liquid holdup
β_2 permanent liquid holdup
ϵ electrode porosity
ϕ inner potential (V)
$\Delta\phi$ voltage drop in the electrode material, $\phi_S(x) - \phi_S(0)$ (V)
μ dynamic viscosity ($kg\,m^{-1}\,s^{-1}$)

Subscripts
G gas phase
L liquid phase
S solid phase

1. Introduction

One of the promising ways of reducing the power consumption in chlor-alkali electrolysis consists of using oxygen reduction

$$O_2 + 2H_2O + 4e^- \rightarrow 4OH^-$$

as an alternative cathodic reaction. The equilibrium cell voltage in brine electrolysis with a hydrogen cathode amounts to 2.2 V under conditions of modern membrane electrolysis (80° C, 34 wt % NaOH in the cathodic compartment and 200 g NaCl dm^{-3} in the anodic compartment), whereas in electrolysis with an oxygen cathode this is only 1.02 V, i.e. 54% less.

Highly effective oxygen gas diffusion cathodes for brine electrolysis based on colloid silver were developed by the Hoechst AG [1–3]. These electrodes were employed in 33% NaOH at 2 to 3 $kA\,m^{-2}$ for more than three years. Similar research was performed at the Case Western Reserve University [4], which resulted in the construction of an experimental membrane electrolyser with an oxygen cathode having an area of 1 m^2 and working with a current loading of 2.5 kA. Electrolyte penetration through the lower part of larger electrodes into the gas compartment was sometimes observed after long term operation. This is a serious problem for an industrial application of gas diffusion electrodes [2]. To avoid this complication, an investigation of another gas electrode, a trickle bed, was initiated. This electrode has been investigated primarily for the purpose of the production of hydrogen peroxide [5–7], although some patents claim its use for brine electrolysis [8, 9].

The trickle-bed oxygen cathode for brine electrolysis has been studied by Oloman and Radcliffe [10] and also in our laboratory [11]. Using ground graphite (0.6–1 mm) in the cathode bed, Oloman and Radcliffe obtained a cell voltage of 2.0–3.0 V at 0.5–1.5 $kA\,m^{-2}$ (10 M NaOH, 70° C, output pressure 0.1 MPa). Better results (2.0–3.4 V at 1 to

0021-891X

3.3 kA m^{-2}) were achieved only by using more dilute catholyte (1.4 M NaOH), higher output pressure (0.77 MPa) and temperatures up to 100° C.

2. Theory

To estimate pressure drop, liquid holdup and mass transfer coefficients in the electrodes studied, equations derived from measurements performed on non-electrochemical trickle-bed reactors are applied (similarly as in Oloman's paper [5]). The two-phase pressure drop (for simultaneous gas and electrolyte flow) was obtained, according to Sato *et al.* [13] by:

$$\Delta P_{GL} = \Delta P_L[1.3 + 1.85(\Delta P_G/\Delta P_L)^{0.425}]^2 \quad (1)$$

Single-phase pressure drop for liquid, ΔP_L, was obtained from the equation [13]:

$$\Delta P_L = (150 + 4.2Re_L^{5/6})\mu_L U_L(1-\epsilon)^2/(d^2\epsilon^3) \quad (2)$$

The gas-phase pressure drop, ΔP_G, was obtained from an identical equation for data pertaining to gas flow. An effective particle diameter, d, which includes the effect of particle roughness on pressure drop, was introduced. It was defined by the equation:

$$d = \bar{d}/f_p \quad (3)$$

The roughness factor, f_p, was estimated by fitting calculated ΔP_L and ΔP_{GL} (according to Equations 1–3) to the measured values.

Transient holdup values come from Specchia and Baldi [14]:

$$\beta_l = 3.86Re_L^{0.545}Ga^{-0.42}(ad/\epsilon)^{0.65} \quad (4)$$

where the modified Galileo number is calculated from

$$Ga = \frac{d^3 h_L(h_L g + \Delta P_{GL})}{\mu_L^2} \quad (5)$$

Mass transfer rates in both the gas phase, $K_G a$, and in the liquid phase between the gas-liquid interface and liquid bulk, $K_L a$, were correlated with energy dissipation related to unit volume (i.e. with the product of pressure drop and fluid velocity), by the Reiss equations [15]:

$$K_G a = 2.0 + 0.069(\Delta P_{GL} U_G)^{0.67} \quad (6)$$

$$K_L a = 0.0173(\Delta P_{GL} U_L)^{0.5} \quad (7)$$

Equation 7 was derived from measurements of oxygen desorption from water at 25° C [15]. In systems with a different value of gas diffusivity, the linear coefficient in Equation 7 must be multiplied by a term $(D/D_0)^{0.5}$, where D_0 is the oxygen diffusivity in water at 25° C [16]. The mass transfer rate between liquid bulk and the liquid-solid interface was calculated from:

$$K_S a = 1.8Re_L^{0.5}Sc_L^{0.33}a^2 D \quad (8)$$

This equation derived by Satterfield [16] for a single-phase flow, was verified by Sato *et al.* for a two-phase flow [17]. The overall mass transfer coefficient was obtained from the equation

$$K_0 = (1/K_G + 1/K_L + 1/K_S)^{-1} \quad (9)$$

based on the simplifying assumption that the gas/liquid and liquid/solid interfacial areas are the same. The mass-transfer controlled limiting current density for oxygen reduction was calculated from

$$j_{lim} = 4Faf_p K_0 c_0 t \quad (10)$$

The validity of the Equations 1–8 for the electrodes studied must be experimentally verified because they were derived from measurements performed on non-electrochemical trickle bed reactors with substantially larger particles (2.9–76 mm).

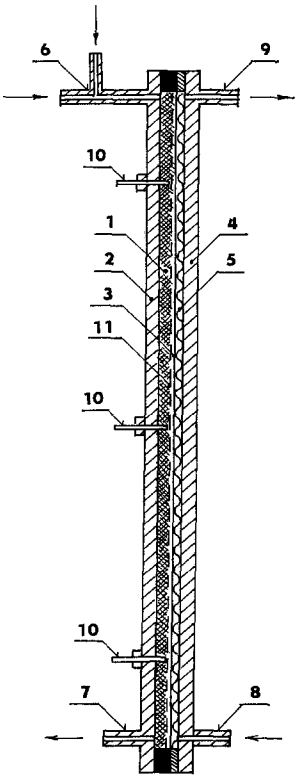

Fig. 1. A cross section of the cell with a trickle-bed electrode.

3. Experimental details

Due to the corrosive properties of chlorine, experimental investigations of an oxygen cathode were performed in an electrolyser with an oxygen anode instead of a chlorine anode. Solutions of sodium hydroxide were used in both the cathodic and anodic compartments.

The electrolytic cell is shown in Fig. 1. Electrode material (1) was compressed between a stainless steel plate (2), which served as a current feeder and an ion-exchange membrane (3). A nickel-plated stainless steel plate (4) together with a fine nickel mesh (5) inserted between the membrane and the plate (4) served as the anode. Electrolyte and oxygen were fed into the injector (6), passed through the trickle-bed electrode, and exited the cell through the tube (7). Anolyte entered the anodic compartment through

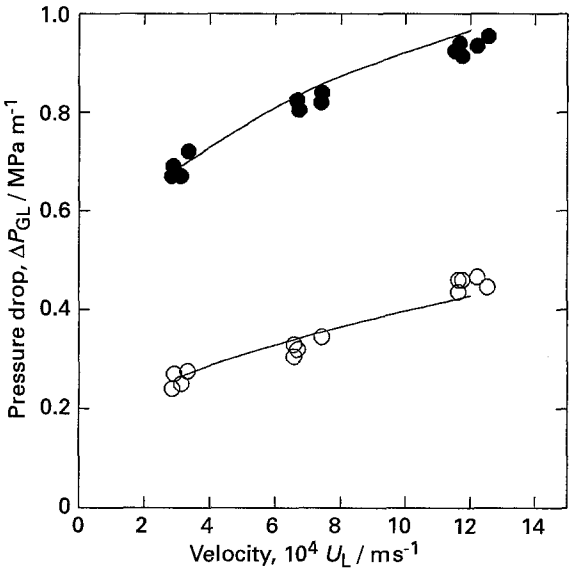

Fig. 2. Effect of electrolyte and gas flow rate on two phase pressure drop in the electrode with 0.18–0.4 mm graphite. $U_G = 0.133\,m\,s^{-1}$ (○) or $0.8\,m\,s^{-1}$ (●), 70° C, one electrolyte circuit (6 M NaOH), output pressure 0.1 MPa. Curves calculated according to Equations 1 and 2 for the values: $f_p = 2.1$, $d = 2.5 \times 10^{-4}$ m, $\epsilon = 0.46$, $h_L = 1190\,kg\,m^{-3}$, $\mu_G = 2.2 \times 10^{-5}\,kg\,m^{-1}\,s^{-1}$, $\mu_L = 1.35 \times 10^{-3}\,kg\,m^{-1}\,s^{-1}$.

the tube (8), and exited through the tube (9). The trickle-bed electrodes were 0.47 m high, 21 mm wide and 3.4 mm thick. The cathode compartment was filled with ground graphitized carbon S 42 (a product of Elektrokarbon Topolčany, Slovakia) with sieve fractions of 0.08–0.18 mm, 0.18–0.4 mm, 0.4–0.63 mm or 0.63–1 mm. Three potential probes (10) made of polyamide (sealed at the end and with four 0.7 mm diameter openings) were used to measure the electrolyte potential relative to the cathode current feeder. The distance x between the probe end and the current feeder was varied. All the measured potentials are reported relative to a mercuric oxide reference electrode in 6 M NaOH. The voltage drop in the layer of electrode material was measured by means of nickel mesh (11) sandwiched between the cathode material and the membrane.

Two types of electrolyte flow were used. The first, with one electrolyte circuit, was characterized by flowing the electrolyte (6 M NaOH) into the anodic compartment and then into the cathodic compartment. The second type of flow had two electrolyte circuits; 6 M NaOH was introduced into the anodic compartment and 0.1 M NaOH into the cathodic compartment. The membrane, Nafion 295 (Du Pont), was used to separate the cathode from the anode compartment. Only Fig. 6 contains results performed with the Volpor diaphragm (Poland). In most experiments, the electrolyte leaving the cathode was at atmospheric pressure (0.1 MPa). The temperature in the electrolyser, usually 70° C, was maintained by means of electrically heated elements fixed to the steel plate of the cathode current feeder.

The transient liquid holdup in the trickle bed electrode, β_1, was determined by measuring the volume

Table 1. Temporary liquid holdup in the electrode with graphite (0.18–0.4 mm) on gas (at atmospheric pressure) and liquid flow rate, 70° C, 0.25 kA m^{-2}, outlet pressure 0.3 MPa. The values in parenthesis were calculated from Equations 1 to 5 with input values given in Fig. 2

U_G/m s^{-1}		*0.133*	*0.8*
$U_L \times 10^3$/m s^{-1}	0.3	0.38 (0.36)	0.26 (0.23)
	0.6	0.46 (0.46)	0.38 (0.32)
	1.2	0.60 (0.60)	0.48 (0.42)

of liquid leaving the electrode for 10 min after discontinuing the current and electrolyte supply while maintaining the oxygen supply. Another type of liquid holdup, referred to in this paper as the permanent holdup, β_2, was determined by the difference between the weight of the wet electrode material after finishing the transient holdup measurement and the weight of this material after it was rinsed and dried. Both the transient and permanent liquid holdups were calculated from the volumes of retained liquid divided by the void volume of the electrode. The total liquid holdup is the sum of its permanent and transient components.

4. Results and discussion

4.1. *Pressure drop*

Single phase pressure drop ΔP_G (with oxygen) and two phase pressure drop ΔP_{GL} (with oxygen and 6 M NaOH) were measured in several beds with different sieve fractions of graphite. It was found that ΔP_G may be approximated satisfactorily by Equation 2 and ΔP_{GL} by Equation 1, if a roughness factor used to calculate an effective particle diameter (Equation 3) had a value of 2 to 2.4 (see Fig. 2). In further calculations (of liquid holdup and of mass transfer), calculated values of ΔP_G, ΔP_L and ΔP_{GL} were used.

4.2. *Liquid holdup*

An example of measured values of transient liquid holdup at different gas and liquid flow rates is shown in Table 1. From this table, it follows that the liquid holdup increases substantially with increasing liquid velocity and decreases with increasing gas velocity. It was found that the liquid holdup at the same gas and liquid mass flow rates is higher at higher pressure. This is due to a lower gas velocity in the electrode at a higher pressure, associated with a lower pressure loss and a lower value of the Galileo number.

A relatively good fit of experimental and calculated values of both two phase pressure drop and transient liquid holdup warrants the use of Equations 1–4, even though these equations were derived from the measurements performed with trickle bed reactors containing substantially larger particles (2.6–25 mm) [13, 14]. The permanent liquid holdup was found to decrease with increasing particle size, from 0.28

Table 2. Calculated two-phase pressure drop and mass transfer rates. Data: $h_L = 1080\,kg\,m^{-3}$, $\mu_L = 7 \times 10^{-4}\,kg\,m^{-1}\,s^{-1}$, $D = 4.2 \times 10^{-9}\,m^2\,s^{-1}$, $c_0 = 0.458\,mol\,m^{-3}$ *(0.1 MPa), 70° C, other data as in Fig. 2*

U_g^0/m s^{-1}	$U_L \times 10^3$ /m s^{-1}	ΔP_{GL}/MPa m^{-1}	K_Ga/s^{-1}	K_La/s^{-1}	K_Sa/s^{-1}	j_{lim} /A m^{-2}
	0.3	0.309	77	0.22	3.97	458
0.19	0.6	0.373	82	0.34	5.62	766
	1.2	0.465	90	0.54	7.95	1306
	0.3	0.707	263	0.33	3.97	1008
0.8	0.6	0.801	268	0.50	5.62	1658
	1.2	0.939	277	0.77	7.95	2786

Table 3. Calculated pressure drop, mass transfer rates and superficial mass transfer controlled current density in electrodes with different particle size. $U_G^0 = 0.8\,m\,s^{-1}$, $U_L = 1.2 \times 10^{-3}\,m\,s^{-1}$, *other data as in Table 2*

d/mm	ΔP_{GL}/MPa m^{-1}	K_Ga/m s^{-1}	K_La/m s^{-1}	K_Sa/m s^{-1}	j_{lim} /A m^{-2}
0.08–0.18	2.70	331	1.30	27.4	10949
0.18–0.40	0.93	277	0.77	7.95	2786
0.40–0.63	0.39	219	0.50	2.86	1003
0.63–1.0	0.21	173	0.37	1.43	542

(sieve fraction 0.08–0.18 mm) to 0.17 (sieve fraction 0.63–1 mm).

4.3. *Mass transfer coefficients*

Mass transfer coefficients were calculated from Equations 6–8, where the pressure drop was calculated from Equation 1. The effect of gas and electrolyte velocity on mass transfer coefficients is shown in Table 2. The symbol U_G^0 represents the oxygen velocity at atmospheric pressure. In the calculations, the arithmetic mean of the data (h_L, μ_L, D, c_0) for input (0.1 M NaOH) and output (6 M NaOH) catholyte were used (the output concentration was estimated from the material balance for a current density 2.5 kA m^{-2} and for a liquid velocity of 6×10^{-4} m s^{-1}). From Table 2 it follows that the rate determining step is the oxygen transfer from the gas-liquid interface to liquid bulk. The gas-phase mass transfer coefficient is higher by more than three orders of magnitude. Higher values of K_S against K_L are probably due to higher gradients of liquid velocity at the liquid-solid interface. As seen from the table, the mass-transfer rate, K_La, increases substantially with increasing liquid velocity and moderately with increasing gas velocity. The mass transfer controlled current density, calculated from Equation 10, increases with gas and electrolyte velocities still more than the mass transfer coefficients. This is a result of the fact that the current density increases, not only due to higher mass transfer coefficients, but also due to a higher mean pressure in the electrode which results in higher oxygen solubility. Calculated values of mass-transfer controlled current density at low gas and liquid flow rates (Table 2) are lower in comparison with the measured current densities (Fig. 5). This indicates that the mass transfer rate is higher than that estimated from Equations 6–8 and so some conclusions described in the following paragraphs may only be taken as semiquantitative.

The calculated mass transfer rate is largely dependent on the particle size (Table 3). With smaller particles, there is a higher pressure drop, which results in higher mass transfer rate. The effect of particle size on mass transfer controlled current density, j_{lim}, is even greater due to the differences in oxygen solubility. This is proportional to the mean pressure which is, at the same outlet pressure, higher in the electrode with smaller particles.

4.4. *Voltage drop in the solid phase*

An electrical resistance of the electrode material the dry state was measured. Values in Table 4 indicate that the specific resistance of the electrode material is substantially lower at higher electrode compression.

Direct measurements of the voltage drop in the solid electrode phase showed that the voltage drop increases with increasing gas and electrolyte flow rates (Fig. 3). In fact, increasing gas flow rate or electrolyte flow rate results in a higher mean pressure in the cathode. Consequently, the pressure difference between the electrode chambers was lower as was the compression of the cathode material. At atmospheric pressure in the anode compartment the cathode was not compressed at all and consequently the voltage drop, $\Delta\phi(t)$ was extremely high (see dashed lines in Fig. 3).

*Table 4. Specific resistance of ground graphite/*Ω *cm*

Fraction/mm	*Compression pressure*/kPa	
	20	*100*
0.18–0.4	1.8	0.5
0.4–0.63	2.4	0.7
0.63–1.0	2.6	0.8

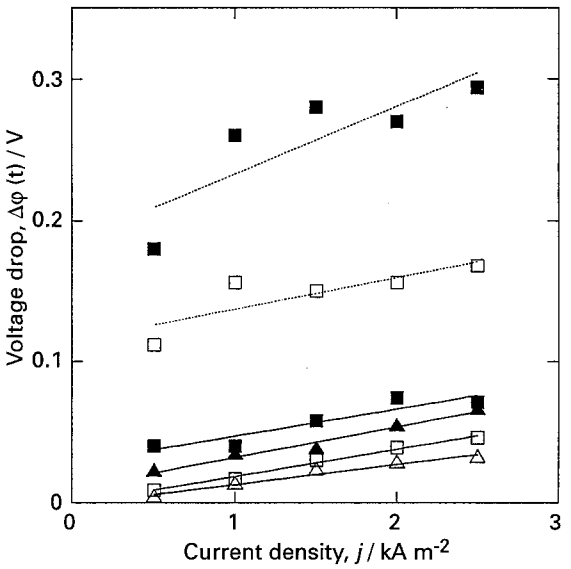

Fig. 3. Average voltage drop in the electrode material against current density. $U_G = 0.133\,m\,s^{-1}$ (△, □), or $0.8\,m\,s^{-1}$ (▲, ■), $U_L = 3 \times 10^{-4}\,m\,s^{-1}$ (△, ▲), or $6 \times 10^{-4}\,m\,s^{-1}$ (□, ■). Pressure in the anode chamber 0.1 MPa (– – –), or 0.36 MPa (——). Two electrolyte circuits, cathodic output pressure 0.1 MPa, 70° C.

4.5. *Potential variation in the trickle-bed electrode*

The measured voltage between the reference electrode and the current feeder consists of a local electrode potential and a voltage drop in the electrode material between the current feeder and the electrode particles near the tip of the potential probe:

$$\begin{aligned} E'(x) &= \phi_S(0) - \phi_L(x) \\ &= [\phi_S(x) - \phi_L(x)] - [\phi_S(x) - \phi_S(0)] \\ &= E(x) - \Delta\phi(x) \end{aligned} \tag{12}$$

With the exceptions of front and back electrode boundaries, the voltage drop in other places, $\Delta\phi(x)$, could not be obtained as the potential probes used could only measure the local potential of the liquid

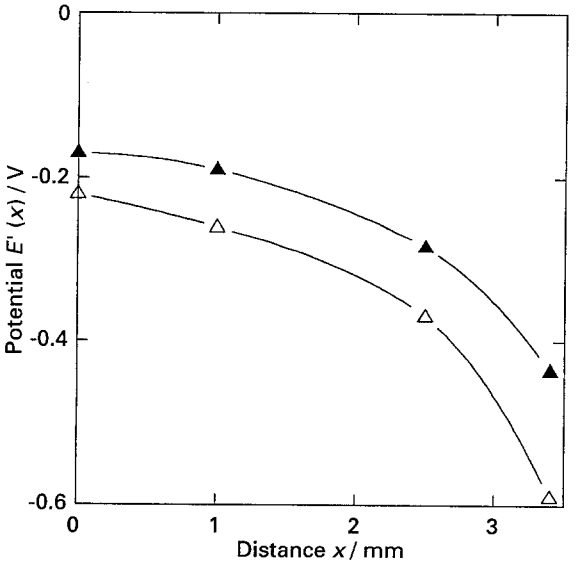

Fig. 4. Variation of the potential $E'(x)$ with the distance from the current collector at $2.5\,kA\,m^{-2}$, $U_G = 0.19\,m\,s^{-1}$(△), or $0.8\,m\,s^{-1}$ (▲), $U_L = 3 \times 10^{-4}\,m\,s^{-1}$. Other data as in Fig. 2.

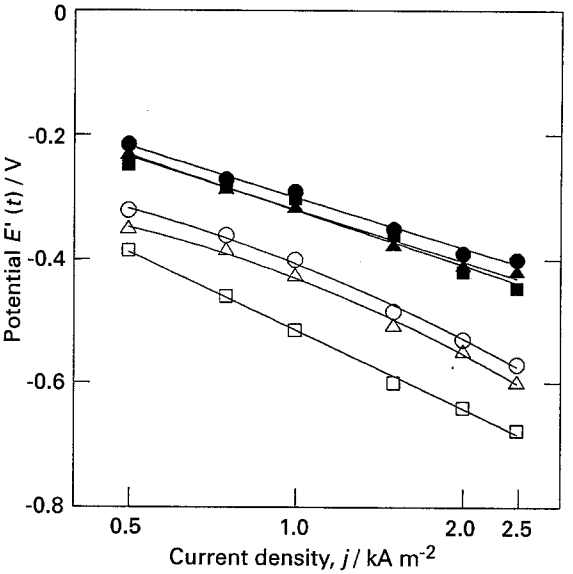

Fig. 5. Polarization curves of trickle electrode. Data: $U_G = 0.19\,m\,s^{-1}$ (△, □, ○), or $0.8\,m\,s^{-1}$ (▲, ■, ●), $U_L = 3 \times 10^{-4}\,m\,s^{-1}$ (△, ▲), $6 \times 10^{-4}\,m\,s^{-1}$ (□, ■) and $12 \times 10^{-4}\,m\,s^{-1}$ (○, ●), other conditions as in Fig. 2.

phase. Therefore only the variation of the potential $E'(x)$ with distance from the current feeder could be evaluated. The potential variation shown in Fig. 4 is caused both by an increase in the voltage drop, $\Delta\phi(x)$, and a negative shift of the local electrode potential, $E(x)$, with x. The evaluation of the potential E at the electrode boundaries has shown that the potential at the membrane, $E(t)$, was always more negative than the potential at the current feeder, $E(0)$. This is typical for porous electrodes with a solid phase conductivity higher than the electrolyte conductivity [18]. The obtained values of $E(0)$ and $E(t)$, however, give no information about the current distribution in the electrode.

4.6. *Polarization curves*

4.6.1. Influence of gas flow rate. To characterize polarization of different trickle bed electrodes, average values of the potential $E'(t)$, measured by three potential probes, were used. An example of polarization curves measured in the electrolyser with one electrolyte circuit is shown in Fig. 5. This figure illustrates that at lower gas flow rates, the potentials are more negative. This coincides with the assumption of the mass transfer controlled process, because with increasing gas flow rate the pressure drop grows as does the mass transfer rate in the liquid phase (Table 2). An additional cause may be the increasing surface area of the gas-liquid interface resulting from higher gas volume in the electrode (Table 1).

Different behaviour should be observed in the case of remarkable current distribution in the electrode, when the reaction is concentrated into a narrow electrode layer. This is the case typical for a charge transfer controlled process. Under this condition, an increase in gas flow rate results in more extreme current distribution, as voltage losses in the electrolyte

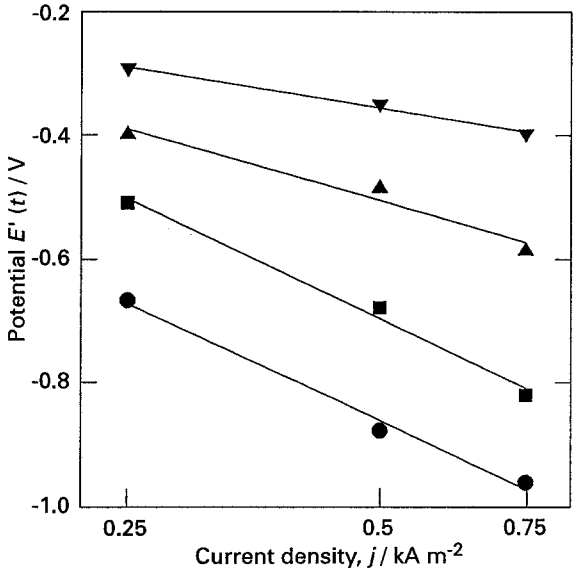

Fig. 6. Polarization curves of electrodes prepared from sieve fractions of graphite: 0.08–0.18 mm (▼), 0.18–0.4 mm (▲), 0.4–0.63 mm (■), 0.63–1 mm (●). Diaphragm Volpor, $U_L = 6 \times 10^{-4}$ m s^{-1} (2 M NaOH), $U_G = 0.33$ m s^{-1}, electrolyser without heating.

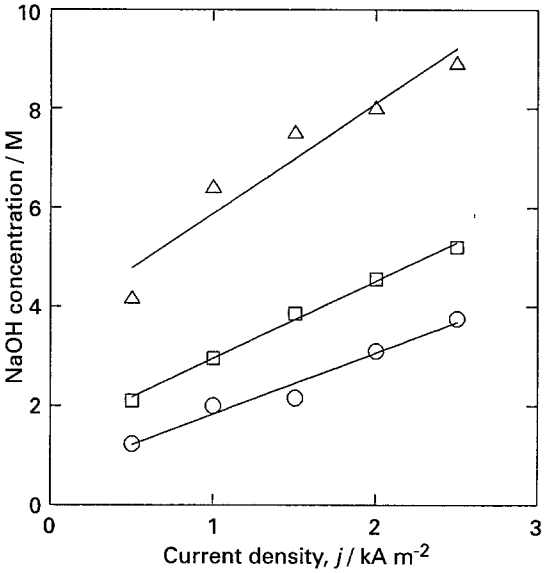

Fig. 7. Effect of current density and electrolyte flow rate on hydroxide concentration at the cathode output. Two electrolyte circuits. Other conditions as in Fig. 5.

increase. This makes the reaction zone narrower and the electrode potential at the membrane more negative. This response however, has not been observed with the electrodes studied.

4.6.2. Influence of liquid flow rate. Figure 5 shows that the electrolyte flow rate has no unambiguous effect on the electrode potential. From Table 2, it is clear that the mass transfer rates increase with increasing electrolyte flow rate. The observed slight, or even opposite, effect of higher liquid flow rate may be explained by decrease of the gas-liquid interfacial area. An increase in electrolyte flow rate lowers the gas proportion in the pores (Table 1) and also the surface area of the gas-liquid interface.

4.6.3. Influence of temperature. Electrode potentials measured at 70° C are substantially more positive (by 0.2 to 0.3 V) than those obtained in the nonheated electrolyser. This is probably a result of the increased oxygen diffusion coefficient [19, 20]. Higher temperatures also increase the electrolyte conductivity, and so reduce the potential variation in the electrolyte. If the current densities in the electrode are lower than the mass transfer controlled limiting current density, higher temperature makes the current distribution more uniform and the electrode potential at the membrane more positive.

4.6.4. Influence of particle size. The measurements performed with electrodes made of different graphite sieve fractions showed that the smaller the particles, the more positive the electrode potential (see Fig. 6). This is caused by higher mass transfer coefficients and by a higher gas-liquid interfacial area in the bed with smaller particles. In the measurements with electrodes made of very fine particles (sieve size less than 0.2 mm) a time dependent increase in the pressure drop was observed and even, in several cases, a plugging of the cathodic output tube.

4.6.5. Influence of electrode compression. The measured potentials, $E'(t)$, were dependent on the compression of the cathode which was determined by the pressure difference between the anode compartment and the cathode bed. At atmospheric pressure in the anode compartment the cathode was not compressed at all and the potential $E'(t)$ was more negative (e.g. at 2.5 kA m^{-2} by 0.36 V than at the pressure of 0.42 MPa in the anode compartment).

4.6.6. Influence of hydroxide concentration. The polarization curves in Fig. 5 were measured with one electrolyte circuit. In this case, the concentration at the cathode output was always constant (6 M NaOH), whereas the concentration at the cathode input (due to the anodic process) decreased with increasing current density and with decreasing electrolyte flow rate (between 0.1 and 5.4 mol dm^{-3}). With two electrolyte circuits, the hydroxide concentration at the cathode input was constant (0.1 M), whereas the output concentration increased with increasing current and with decreasing catholyte flow rate (see Fig. 7).

A substantial decrease in oxygen solubility with increasing alkali hydroxide concentration [20, 21] explain the different shape of the polarization curves in Figs 5 and 8. With one electrolyte circuit a lower liquid flow rate results in a lower mean hydroxide concentration in the catholyte and, consequently, a higher oxygen solubility. This counterbalances the negative effect of the lower liquid flow rate on mass transfer coefficients so no unambiguous effect of liquid flow rate on the electrode potential is observed (Fig. 5). With two electrolyte circuits, a lower catholyte flow rate results in both lower mass-transfer coefficients

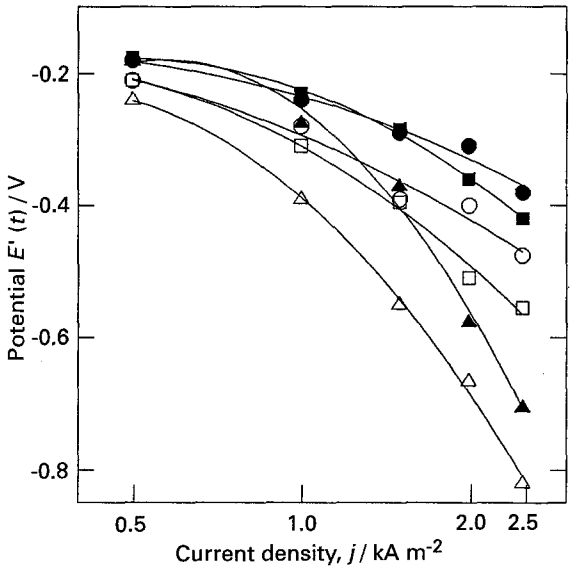

Fig. 8. Polarization curves of electrode with two electrolyte circuits. Description and other conditions as in Fig. 5.

and lower oxygen solubility. Therefore, a significant negative potential shift is observed.

5. Conclusions

It was shown that oxygen reduction in the trickle bed electrodes studied is controlled mostly by the transport of oxygen in the liquid phase between the gas-liquid interface and liquid bulk. This explains the experimentally found effects of gas and liquid flow rates, temperature, particle size and hydroxide concentration on the electrode potential. It was found that compression of the cathode material is necessary for proper operation. The activity of these electrodes increases substantially with decreasing particle size of the electrode material.

The potential (measured at the membrane against the current collector) of the electrodes studied is, at current densities of 2–2.5 kA m^{-2} and at output hydroxide concentrations of 4–5 mol dm^{-3}, above the potential of loaded low-overvoltage cathodes for hydrogen evolution [21] by 0.57–0.63 V. At higher hydroxide concentrations, however, the potential is shifted to more negative values.

In comparison with gas diffusion electrodes, the potential of trickle-bed electrodes is more negative. This reflects the fact that the three phase boundary in gas diffusion electrodes is increased and that the rate of oxygen transport through a thin electrolyte film near this boundary is higher than through a thicker liquid layer in trickle-bed electrodes.

Acknowledgement

The author is indebted to his colleagues Ing. Karel Balogh and Ing. Milada Thumová for extensive experimental work and to Carla Gracey for her assistance in editing the manuscript.

References

[1] R. Staab, *German Patent 3 303 779*, 4 Feb. 1983, Hoechst AG.
[2] R. Staab, *Chem.-Ing.-Tech.* **59** (1987) 316.
[3] K. H. Tetzlaff, *US Patent 5 104 497*, 14 Apr. 1992, Hoechst AG.
[4] Cited by V. H. Thomas and E. J. Rudd, *in* 'Modern Chlor-Alkali Technology', Vol. 2, (edited by C. Jackson), E. Horwood, Chichester (1983) p. 168.
[5] C. Oloman and A. Watkinson, *J. Electrochem. Soc.* **126** (1979) 1885.
[6] J. B. Davison, J. M. Kaczir, P. J. Peerce-Landers and R. Jasinski, *J. Electrochem. Soc.* **130** (1983) 1497.
[7] O. Špalek and K. Balogh, *Coll. Czech. Chem. Commun.* **54** (1989) 1564.
[8] O. De Nora and L. Pellegri, *US Patent 4 177 116*, 4 Dec. 1979, De Nora Implanti Electrochimica.
[9] J. A. McIntire and R. F. Phillips, *US Patent 4 224 192*, 23 Sept. 1980.
[10] C. Oloman and J. Radcliffe, *J. Appl. Electrochem.* **16** (1986) 457.
[11] O. Špalek and I. Paseka, *in* Proceedings 'Perspektivy výroby chloru a alkálií v ČSSR', Jetřichovice (1984) p. 43.
[12] O. Špalek, *Collect. Czech. Chem. Commun.* **51** (1986) 1883.
[13] Y. Sato, T. Hirose, I. Takahashi and M. Toda, *J. Chem. Eng Jpn.* **6** (1973) 147.
[14] V. Specchia and G. Baldi, *Chem. Eng. Sci.* **32** (1977) 515.
[15] L. P. Reiss, *I&EC Process Des. Dev.* **6** (1967) 486.
[16] Ch. N. Satterfield, *AIChE J.*, **21** (1975) 209.
[17] Y. Sato, T. Hirose, F. Takahashi and M. Toda, Pacific Chem. Eng. Conf., Session 8, pap. 8–3, (1972) 187.
[18] D. J. Picket, 'Electrochemical Reactor Design', Elsevier, New York (1977) p. 234.
[19] M. K. Tham, R. D. Walker and K. E. Gubbins, *J. Phys. Chem.* **74** (1970) 1747.
[20] R. E. Davis, G. L. Horvath and C. W. Tobias, *Electrochim. Acta* **12** (1967) 287.
[21] Cited by D. E. Brown, P. O. Fogarty, M. N. Mahmood and A. K. Turner, *in* 'Modern Chlor-Alkali Technology', (edited by C. Jackson), Ellis Horword, Chichester (1983) p. 240.